IEEE Access
Multidisciplinary ⋮ Rapid Review ⋮ Open Access Journal

Received April 28, 2020, accepted May 19, 2020, date of publication May 22, 2020, date of current version June 11, 2020.

Digital Object Identifier 10.1109/ACCESS.2020.2996969

Modeling and Fault Categorization in Thin-Film and Crystalline PV Arrays Through Multilayer Neural Network Algorithm

AZHAR UL-HAQ[1], HATEM F. SINDI[2], (Member, IEEE), SABA GUL[1], AND MARIUM JALAL[3,4]

[1]Department of Electrical Engineering, College of EME, National University of Sciences and Technology (NUST), Islamabad 44000, Pakistan
[2]Electrical and Computer Engineering Department, King Abdulaziz University, Jeddah 21589, Saudi Arabia
[3]Department of Electrical Engineering, Fatima Jinnah Women University, Rawalpindi 46000, Pakistan
[4]Department of Electrical Engineering, Lahore College for Women University, Lahore 54000, Pakistan

Corresponding author: Azhar Ul-Haq (azhar.ulhaq@ceme.nust.edu.pk)

This project was funded by the Deanship of Scientific Research (DSR), King Abdulaziz University, Jeddah, under grant No. (D-639-135-1441). The authors, therefore, gratefully acknowledge DSR technical and financial support.

ABSTRACT Categorization of PV faults is an essential task for improving the efficiency and reliability of a photovoltaic (PV) system. Output characteristics of a solar (PV) system can be severely affected under various fault conditions including short circuit, module mismatch, open circuit, and multiple faults under shading conditions. Such PV faults can potentially be analyzed through the PV characteristic curve analysis using a multilayer neural network with a scaled conjugate gradient algorithm (SCG). This paper presents an extensive investigation for categorization, i.e., classification of the above-mentioned PV faults using the SCG algorithm. The major contribution of the presented research work is the categorization of PV faults in sixteen different classes considering polycrystalline and thin-film PV technologies with two different configurations, including SP and TCT. The fault classification is achieved with high accuracy of 99.6% and a fast-computational time of 0.08 sec. The results are validated through the plot of the Confusion Matrix and Region of Convergence (ROC) with their performance evaluation in MATLAB. The achieved accuracy and fast computational time prove the effectiveness of the multilayer neural network-based approach for classification of the PV faults to increase power output, efficiency, and lifespan of PV systems.

INDEX TERMS PV faults, PV technologies, PV characteristics, neural networks.

I. INTRODUCTION

A massive body of research has been focused on the advancement of solar photovoltaic (PV) technology with an aim to improve the latter's efficiency and high variability due to its non-linear nature and high reliance on external atmospheric conditions [1]. The high sensitivity of PV systems to extreme weather conditions such as thunderstorms, rain, and humidity, high ambient temperatures, and non-uniform shading can severely impact the output characteristics of PV arrays, which are connected in various configurations for harnessing of maximum power output [2]. Various interconnections of PV modules can develop severe internal faults like an open and short circuit, and hotspot heating under uncertain environmental conditions, which can lead towards blackout of the entire PV system [3]. Therefore, early detection and timely diagnosis of faults are necessary to prevent extraordinary power losses and reliable operation of PV arrays.

In this regard, the classification of PV faults has been reported in the literature for the proper diagnosis of faults and to increase the life span of a PV power system. Different fault detection techniques for recognition of PV arrays faults have been reported in the literature works like time domain reflectometry [3] and earth capacitance measurement [4]. Online fault diagnostic technique through infrared imaging has been used for fault identification in [5] that differentiates faulty PV modules from normal module through change in apparent temperature. Authors in [6], [8], and [9] attempted to figure out the location and type of fault by collection of data through installation of current and voltage sensors on small PV arrays, but those techniques do not effectively detect the faults in large PV systems. Time Domain

The associate editor coordinating the review of this manuscript and approving it for publication was Zhehan Yi.

This work is licensed under a Creative Commons Attribution 4.0 License. For more information, see https://creativecommons.org/licenses/by/4.0/

Reflectometry (TDR) is an effective technique for PV fault diagnosis in a series-connected PV farms. However, it requires precision instrument for analysis of signals to diagnose the fault accurately and can only be applied to series-connected PV modules as presented in [6].

As mostly PV arrays are connected in various series-parallel configurations to extract the required amount of power, techniques presented in the above-cited works cannot diagnose faults in series-parallel configurations of PV arrays. Many investigations by various authors have been conducted to analyze environmental impact like severe shading on various series-parallel topologies [7]–[10]. It is known that the impact of fault can vary upon the form of interconnection and type of PV technology. The impact of different PV arrays' faults on different configurations include as given in [11]–[16]: Honey Comb (HC), Total Cross Tied (TCT), and Bridge Linked (BL) have been investigated with consideration of thin-film and monocrystalline PV arrays. Authors in [16] restrict the investigated impact of open circuit, short circuit, and shading fault on a reasonably small 6×6 PV array. Power loss minimization has been achieved in [11] with thin-film PV technology under various faulty scenarios with power-voltage (P-V) curve analysis only. From the given literature, it is found that there is room to investigate different PV faults' impact on different PV materials with the larger interconnected PV arrays through analysis of both P-V and I-V curves. It is pertinent to mention that the I-V curve is considered more crucial for the recognition and classification of PV faults in a PV system.

In fact, faults in an interconnected PV array are challenging to diagnose due to their unpredictability and non-linearity. Artificial neural networks (ANN) can, fortunately, characterize the relationship between input states and expected output with complex structure, connecting weights, bias, and thresholds. The probabilistic neural network (PNN) has been used in [12], which classifies different PV faults with 85% precision. Accuracy of the computed results is necessary for the proper diagnosis and categorization of such faults. It is believed that fault classification through artificial neural networks (ANN) can be a good solution in terms of accuracy, fast computation, and ease [13]. In [14], a neural network model was designed to envisage the output power of PV modules. The neural network (NN) was used for categorization of different PV faults in [15], but none of the studies have categorized and classified diverse faults of TCT, BL and SP interconnected PV arrays in different PV materials [15] with high precision and accuracy through ANN as summarized in Table 1. In particular, classification of multiple faults in thin-film and crystalline PV technologies remain unveiled in the literature.

To bridge the aforementioned research gap, the presented research work investigates various topologies, including SP, TCT, and BL, and gives its detailed analysis through I-V and P-V characteristics curve. Two different PV technologies, including thin-film and polycrystalline PV, have been considered for this analysis. An extensive input data set of 5×1248 has been developed and collected by computation and analysis of change in the output of the considered interconnected PV arrays. The performance of PV arrays is analyzed with classification and recognition of the PV faults through the backpropagation algorithm of neural networks. The adapted procedure recognizes all the faults with high accuracy and categorizes the faults with respect to different PV materials. The contributions of this research work are as follows:

1. Different types of faults in PV arrays are analyzed on a thin-film and crystalline 9×7 PV array to investigate the faults' impact on the characteristics curve of a PV system. The combined impact of faults is also analyzed on TCT, BL, and SP interconnection of the PV array.
2. All faults are categorized and classified through a multilayer neural network with high accuracy of 99.6% and a faster computation time of 0.08 sec than that of the literature works [12]. This research has also classified all simulated faults in PV array with differentiation of different PV materials, including thin-film and crystalline technology, which is not reported in the literature.
3. PV faults are categorized into two different PV configurations, including SP and TCT, through neural networks with high accuracy of 99.6%, which is not achieved in the previous research works. Thermal imaging for feature extraction is used in [17] with NN as a classifier for fault detection in PV modules, which achieved 92.8 % overall accuracy as a fault classifier. A comparison of NN classifier with conventional classifiers like K-nearest neighbor (KNN), and support vector machine (SVM) is also made in [17]. Classifiers like SVM and KNN achieved an accuracy of 80.3% and 56.8% respectively, while NN classifier performed better as a fault classifier and achieved an overall accuracy of 92.8% in classification of faults in the PV module. Accurate detection of shading fault in PV systems is performed through principal component analysis (PCA) with achieved average accuracy of 97% in [18]. Convolutional NN based approach is used in [19] for extraction of features from scalograms and to perform classification of faults with 73.5% accuracy without considering different PV materials. PV faults were categorized with 99% accuracy without consideration of PV material and configuration of PV array in [16]. Classification of open and short circuit faults in a PV array through PNN is achieved in [20] with an accuracy of nearly 98%. Diagnosis of various faults has been conducted through various methods, including I-V measurements with machine learning techniques and multiclass exponential loss function (SAMME-CART) in references [21]–[24]. Over 95% average accuracy is achieved in classification of each fault. None of the previous research works has classified PV module mismatch, open and short circuit, multiple faults under shading conditions in different PV materials and configurations with 99.6% accuracy and fast computational time [26]–[32].

TABLE 1. Literature survey and identification of gaps.

Proposed Work	Technique	Contribution	Research Gap
[5]	Infrared imaging for fault identification in PV modules	Locate and identify faults through capturing apparent temperature difference in module with an infrared camera	• Only for small PV systems • Need infrared cameras • Not accurate
[9] [17]	Multi-sensor technique for identification of PV faults	Locate and identify faults	• Need installation of sensors • Only for small PV systems
[3]	Time domain reflectometry (TDR)	More effective and accurate than infrared imaging and multisensory technique	• Only for series-connected modules • Cannot identify a fault in series-parallel configurations of PV array
[4] [6]	Capacitance to ground measurement procedure	More effective than infrared imaging and multisensory technique Accurate and precise	• Only for series-connected modules • Cannot identify a fault in series-parallel configurations of PV array
[24]	Satellite observations for failure detection in the PV system	Detect faults through the collection of climatic data	• Needs climatic and satellites data • Expensive to implement
[12]	Probabilistic neural network (PNN)	85% precision achieved in fault identification through a neural network	• Need large data set
[14]	Neural Network (NN) for prediction of power output	Predict the power output of PV modules with accuracy	• Need large data set • Only power of normal PV module is predicted
[15]	Neural Network for Monitoring of Photovoltaic Panel	Monitor the PV system with accuracy and precision	• Need large data set • Only for monitoring of system
[25],[26]	NN for fault classification	Accurate and precise for fault identification	• Need large data set • Need further research to identify a fault in different configuration • Need to classify faults in different PV technologies with higher precision and accuracy

4. An extensive input data set of 5 × 1248 is collected through analysis and computation of parameters of thin-film and polycrystalline PV arrays. Five input parameters are considered with each input having 1248 samples for the classification of faults through NN algorithm with high accuracy of 99.6%.
5. The results are validated through plotting the best validation performance, confusion matrix, and region of convergence (ROC) analysis for the classification of faults in dissimilar PV technologies, i.e., thin-film and crystalline.

The rest of the article is organized as follows: mathematical modeling of the developed system is explained in Section-II.

SCG algorithm is explained in Section-III. Obtained results and computations are detailed in Section-IV. The conclusion is given in Section-V.

II. SYSTEM MODELING

Two different PV arrays are considered for the classification of faults, including p-n hetero-junction (thin-film; amorphous silicon) and p-n homo-junction. The five-parameter model is selected over the seven-parameter model due to higher accuracy for fault analysis in crystalline PV array, as depicted in Figure 1 in which a single PV cell is coupled in parallel to one diode as a current (I_L) source [11].

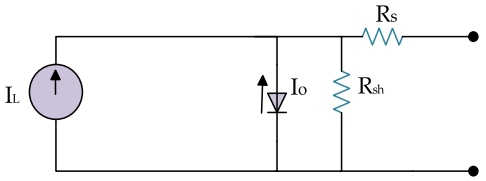

FIGURE 1. Five parameter equivalent PV Model.

The shunt resistance and series resistance are characterized by R_{sh}. and $R_{s,}$ respectively. n is an ideality factor. The value of I_{sc} signifies short circuit current. T_R represents working temperature, while T_{STC} is the temperature at standard testing condition, i.e., 25°C. The coefficient of I_{sc} and V_{oc} are articulated as k_i and k_v, respectively. The irradiance at STC is denoted by G_{STC}. N_{sr} *and* N_{pa} are total number of series cells and parallel PV cells, respectively. The semiconductor's energy bandgap is signified by E_{go}. The output current of PV module is represented by $I_{output,}$ as found in Eq. (1).

Thermal voltage, open-circuit voltage, and short-circuit current are characterized by V_t, V_{oc} and I_{sc}, respectively as given in Eqs. (2) & (3) [33, 34]. I_{STC} and V_{STC} are current and voltage at STC, while G_R is the irradiance.

Homojunction cells follow superposition theorem. Authors in [23] adopted an analytical model of heterojunction solar array, which computes current and voltage parameters of a PV cell, denoted by J and V, respectively. The a-Si cells use a triple layer *p-i-n* form of structure having thick p-n layer and i-layer of nearly 1 micrometers thickness. The voltage-dependent charge collection is the most dominant charge collection mechanism. An analytical expression is obtained for voltage-dependent photocurrent in [23] to describe current J voltage V characteristics in thin-film cell. Total current density is denoted as follows in Eq. (4). J_d and J_L represent forward diode current and photocurrent density, respectively. The total photocurrent density $J_L(\lambda, V)$ represent the sum of current density for the carriers drifting towards the bottom contact $J_b(\lambda, V)$ and the current drifting towards the top contact $J_t(\lambda, V)$ as given in Eq. (5) and Eq. (6). Where Δ is a normalized absorption depth, τ_b and τ_t are normalized carrier for drifting towards bottom and carrier drifting towards the top contact, respectively. Total photo-generated density is found by integrating overall incident photon's wavelength of spectrum as follows in Eq. (7). Modeling of different PV materials is explained for describing the diverse behavior of PV materials under fault conditions due to their different material composition.

$$I_{output} = N_{pa} \times ([I_{sc} + k_i(T_R - T_{STC})]G_{STC}) - N_{pa} \times I_o \times \left[\left[\exp\left(\frac{\frac{V}{N_{sr}} + \frac{I_{output} \times R_s}{N_{pa}}}{n \times V_t}\right) - 1\right] - \frac{V \times \frac{N_{pa}}{N_{sr}} + I_{output} \times R_s}{R_{sh}}\right] \quad (1)$$

$$I_{sc} = N_{pa}\left(\frac{I_{STC}}{G_{STC}} \times G_R + k_i(T_R - T_{STC})\right) \quad (2)$$

$$V_{oc} = N_{sr}(V_{STC} + k_v(T_R - T_{STC}) + V_t \times \ln\left(\frac{I_{sc}/N_{pa}}{I_{STC}}\right) \quad (3)$$

$$J(V) = J_d(V) - J_L(V) \quad (4)$$

$$J_L(\lambda, V) = J_b(\lambda, V) + J_t(\lambda, V) \quad (5)$$

$$J_L(\lambda, V) = eGW\left\{\left(\tau_b^{-1} - \Delta^{-1}\right)^{-1}\left[\Delta\left(1 - e^{\frac{-1}{\Delta}}\right) - \tau_b\left(1 - e^{\frac{1}{\tau_b}}\right)\right] + \left(\tau_t^{-1} + \Delta^{-1}\right)^{-1} \times \left[\Delta\left(1 - e^{\frac{-1}{\Delta}}\right) - \tau_t\left(e^{\frac{-1}{\Delta}} - e^{\frac{-1}{\Delta} - \frac{1}{\tau_t}}\right)\right]\right\} \quad (6)$$

$$J_L(V) = \int_0^{\infty} j_L(\lambda, V)d\lambda \quad (7)$$

A. DEVELOPED FAULTS IN PV ARRAY

All developed faults are analyzed in three configurations, including BL, SP, and TCT. The SP is widely used interconnection of PV arrays. The BL interconnection is also a type of SP interconnection with more internal interconnections than SP in a design like bridge formation, and TCT in which PV modules are joint together, as shown in Figure 2.

A Simulink model of a 9 × 7 PV array under electrical faults is developed to study the performance of faulted PV array, as shown in Figure 3. Four different fault scenarios are analyzed in this study, including module mismatch (F1), short circuit (F2), open circuit (F3), and combined impact of faults in case of multiple faults scenario (F4).

Module mismatch fault (F1): Module mismatch fault is analyzed in this case, which is developed by the provision of non-uniform irradiance to designed 9×7 PV array, as revealed in Figure 4. Temperature of PV components due to heating and non-uniform irradiance is also analyzed through applying 35°C (more than STC 25°C) to first, second parallel string, and 38°C to fourth, fifth, sixth and seventh parallel PV string, respectively. A 9 × 7 PV array is considered a non-square matrix due to unequal number of rows 'm', and column 'n'.

Where element '11' denotes row '1' with column '1', i.e., PV module '1' in column '1' or first parallel string. The '31' refers to third PV module in first parallel string.

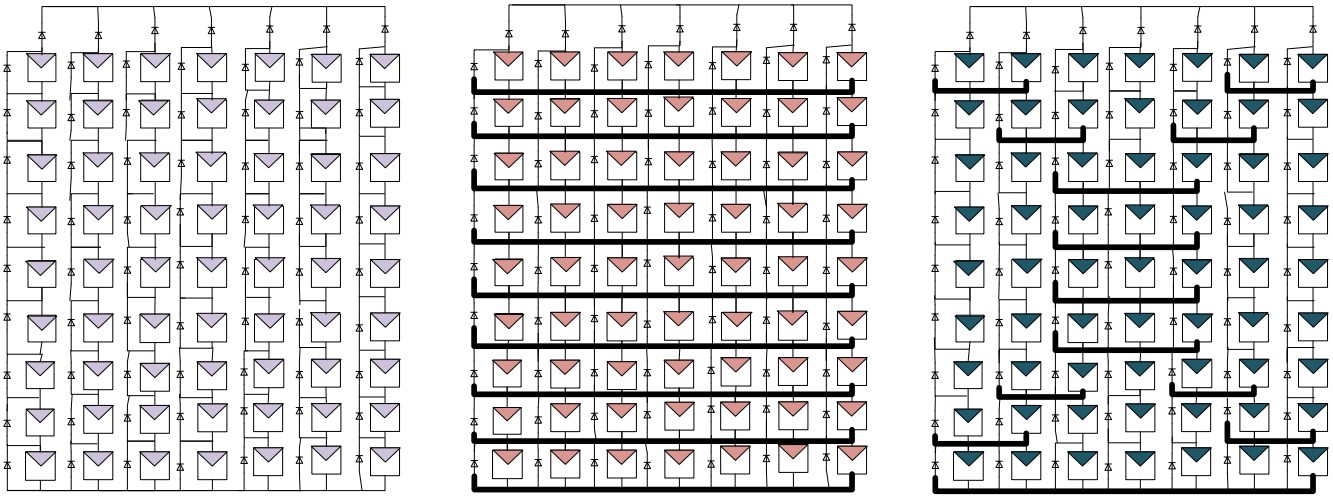

FIGURE 2. (a) SP, (b) TCT, (c) BL topology.

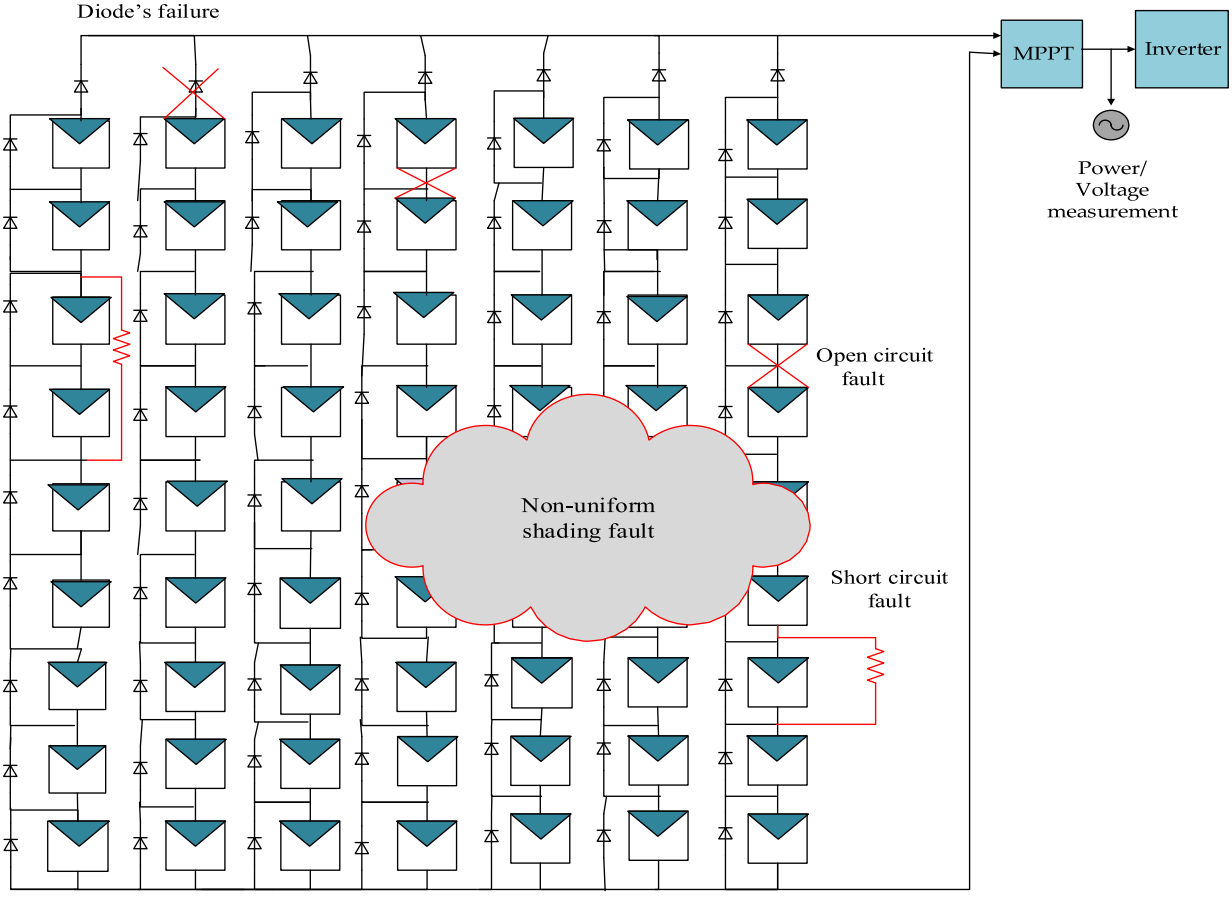

FIGURE 3. Fault analysis in developed PV model.

Sudden decrease in current and voltage is encountered due to non-uniform shading, which indicates a severe impact of low irradiance and high temperature on PV array. The change in values of current and voltage reduces the power significantly. The thin-film PV technology has less severe impact on the performance of the system due to decrease in current loss.

Short circuit fault with bypass diode failure (F2): This fault case is observed by introducing short circuit fault between modules in the PV string. Bypass diode failure is also

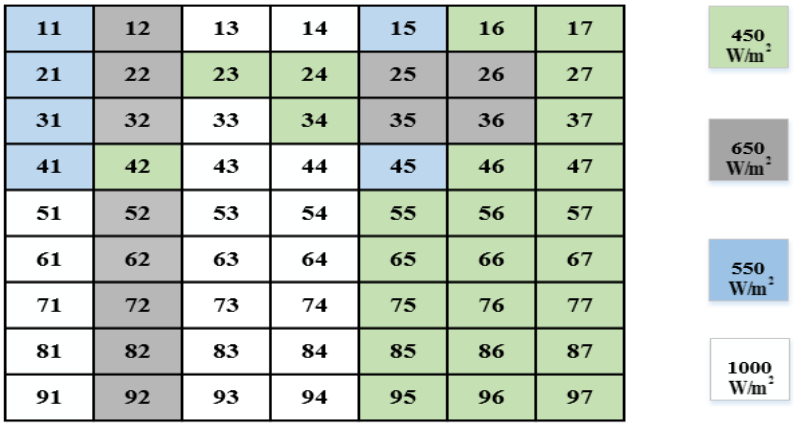

FIGURE 4. Non-uniform shading pattern for 9 × 7 PV array.

analyzed by developing short circuit fault with diode connection. The peak voltage and peak current reduce the power output significantly after occurrence of short circuit fault in the PV array. The usage of thin-film PV can optimize the system's performance, but power loss still occurs in the both PV arrays. The occurrence of short circuit fault indicates significant change in current, voltage, and power of PV system.

Open Circuit (F3): This fault appears due to loose connection of modules leading to module disconnection, which is analyzed in terms of decrease in current, voltage, and power of PV array.

Multiple Faults (F4): All developed faults are analyzed under shading for investigation of the combined effect of PV faults upon the adopted interconnected PV arrays. Sudden decrease in current and voltage are indicated due to occurrence of faults under low irradiance and high-temperature conditions. The details in change of PV parameters after occurrence of each fault are detailed in the section of results. The samples of the affected PV parameters like current, voltage, power, irradiance, and temperature are also collected for classification of PV faults.

The characteristic parameters of a PV array-like irradiance, temperature, short circuit current, open circuit voltage, and peak power are analyzed under the different fault scenarios, and a novel data set of 5 × 1248 is developed after analyzing and computing 1248 samples of 5 inputs. The proposed method can classify faults in sixteen different classes through categorization of faults after applying SCG algorithm of multilayer neural network. In order to classify the faults accurately, we need to select feature quantities that can characterize and recognize the fault signal accurately. The input data set of 5 × 1248 correspond to 5 PV parameters (features of fault signal to perform fault categorization). Each PV parameter has 1248 samples that characterize the different classes of faults. A 16 × 1248 target data set correspond to 1248 associated class vectors defining which of sixteen classes each input is assigned to. Flow chart of the adopted method is depicted in Figure 5. The multilayer NN uses SCG as a training algorithm for the categorization of faults, which updates the weight vectors after comparing output with target data set of 16 × 1248. It computes the minimum global error, which is used for accurate classification of faults through computation of confusion matrix. The cross-entropy (CE) is computed to check the performance. The algorithm successfully classifies the faults in TCT and SP type of interconnected PV arrays with categorization in thin-film and crystalline PV array, as shown in Figure 6.

III. SCG ALGORITHM OF NEURAL NETWORK

Fast-supervised learning algorithm of scaled conjugate gradient (SCG) for PV fault classification is used in this multilayer algorithm which adjusts the weights in the steepest descent direction (negative of the gradient) and avoids the line search per learning iteration in order to scale the step size. A backpropagation method is used in this study with SCG as a training algorithm. Three layers, including hidden layer, input and output layers, constitute the structure of this network. The input layer propagates the data forward to the output layer known as forward propagation. A total of five inputs, each having 1248 samples propagate to hidden layer of 10 neuron layers to update weights and biases at each iteration. Total five inputs, including temperature, irradiance, open-circuit voltage short circuit current,, and temperature, are used in the input layer. Minimum squared error (MSE) is computed from the output through the developed network. The error is calculated based on difference between predicted and actual outcomes. The derivative of error is computed w.r.t each weight in the network to back propagate the error and update the model after minimizing the error. The same process is repeated multiple times to learn ideal weights. The network also includes hidden layer of ten neurons and output layer representing sixteen outputs, which are classifying the faults. Each layer has the tangent sign as the activation function known as sigmoid function. The sigmoid function is used for classification of faults, which constraints the output between 1 and 0. The error is computed by comparing estimated

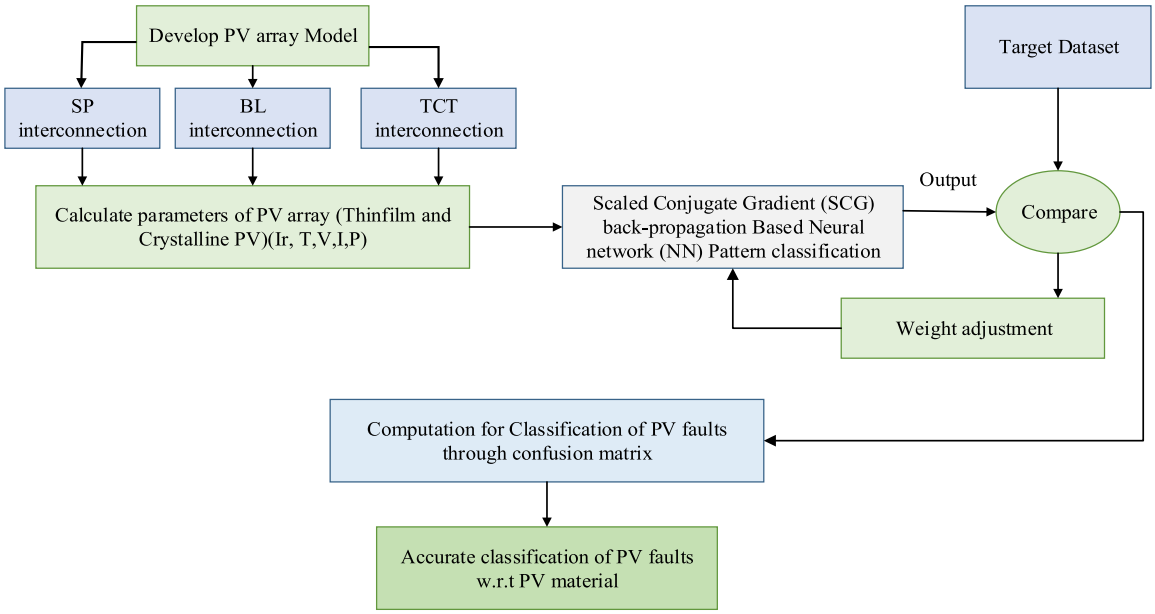

FIGURE 5. Flow diagram of the developed scheme.

output to the real output, and then biases and weights are updated accordingly. The values close to 0 are desirable for estimating correct output. The cross-entropy is a loss function for classification problems. The process can be repeated for specific iterations until global minimum error is achieved.

This SCG algorithm is shown in Figure 7. Let $\tilde{w}$ be the weight vector and global error function $\tilde{E}$. $\tilde{E}$ might be an appropriate error function which can be calculated with one forward pass and the gradient $\tilde{E}'$ with one forward and one backward pass. where 'p' is the number of patterns during training, and E_p is the error. The term $\tilde{s}_n = E^{''}(\tilde{w}_k)\,\tilde{p}_k$ is estimated with a non-symmetric approximation as in Eq. (4) [18].

$$\tilde{s}_k = E^n(\tilde{w}_k)\tilde{p}_k \approx \frac{E'(\tilde{w}_k+\sigma_k\tilde{p}_k)-E'(\tilde{w}_k)}{\sigma_k}, \quad 0<\sigma_k \ll 1 \tag{8}$$

The approximation inclines to the true value of $E''(\tilde{w}_k)\,\tilde{p}_k$. The complexity in computation is $O(3N^2)$ and $O(N)^5$, and all this is combined with Conjugate gradient (CG) approach to get fast computation and more accuracy [18].

The CG approach is combined with model trust region approach termed as Levenberg-Marquardt algorithm for this algorithm. The S_k indicates second-order information. It is computed as follows in Eq. (5).

$$\tilde{s}_k = \frac{E'(\tilde{w}_k + \sigma_k\tilde{p}_k) - E'(\tilde{w}_k)}{\sigma_k} + \lambda_k\tilde{p}_k \tag{9}$$

If sigmoid function $\delta_k \leq 0$ in given iteration, then the raise in λ_k is determined by Eq. (6). The raise in λ_k occurs and $\tilde{s}_k$ is estimated again as $\bar{\tilde{s}}_k$.

$$\delta_k = \tilde{p}_k^T\bar{\tilde{s}}_k = \delta_k + (\bar{\lambda}_k - \lambda_k)\tilde{p}_k^T > 0 \rightarrow \lambda > \lambda_k - \frac{\delta_k}{|\tilde{p}_k|^2} \tag{10}$$

This Eq.(6) implies that if λ_k is more then $-\left(\frac{\delta_k}{|\tilde{p}_k|^2}\right)$, then $\delta_k > 0$. The value of $\bar{\lambda}_k$ depends upon Eq.(7) to get an optimal solution.

$$\bar{\lambda}_k = 2\left(\lambda_k - \frac{\delta_k}{|\tilde{p}_k|^2}\right) \tag{11}$$

$$\bar{\delta}_k = \delta_k + \left(\lambda_k - \bar{\lambda}_k\right)|\tilde{p}_k|^2 \tag{12}$$

$$\alpha_k = \frac{\mu_k}{\delta_k} = \frac{\mu_k}{\tilde{p}_k^T\tilde{s}_k + \lambda_k\,|\tilde{p}_k|^2} \tag{13}$$

A comparison parameter (CP) is introduced to raise and lower the value of scale parameter (SC), i.e., λ_k for good approximation, even with a positive definite Hessian matrix. The values of λ_k directly increases the step size in such a way that the bigger value of λ_k makes the step size smaller. The step size Δ_k is found to be in Eq. (10).

$$\mathrm{CP} = \Delta_k = \frac{2\delta_k\left[E(w_k) - E(\tilde{w}_k + \alpha_k\tilde{p}_k)\right]}{\mu_k^2} \tag{14}$$

The Δ_k is a comparison parameter (CP) whose value is close to 1. If CP is less than 0.25, then scale parameter (SC) is found in Eq. (11).

$$\mathrm{SC} = \lambda_k = \frac{\lambda_k + (\delta_k\,(1-\Delta_k))}{|\tilde{p}_k|^2} \tag{15}$$

If the steepest direction is not equal to zero, then set $k = k + 1$ and update weight vectors otherwise terminate and return the $\tilde{w}_{k+1}$ as desired and required minimum weight. This scale parameter should be greater than zero for a successful reduction in error. SCG algorithm does not involve user-dependent parameters as described in algorithm, which is significant advantage in comparison to line-search based algorithms. The samples are divided randomly in which 70% samples are used

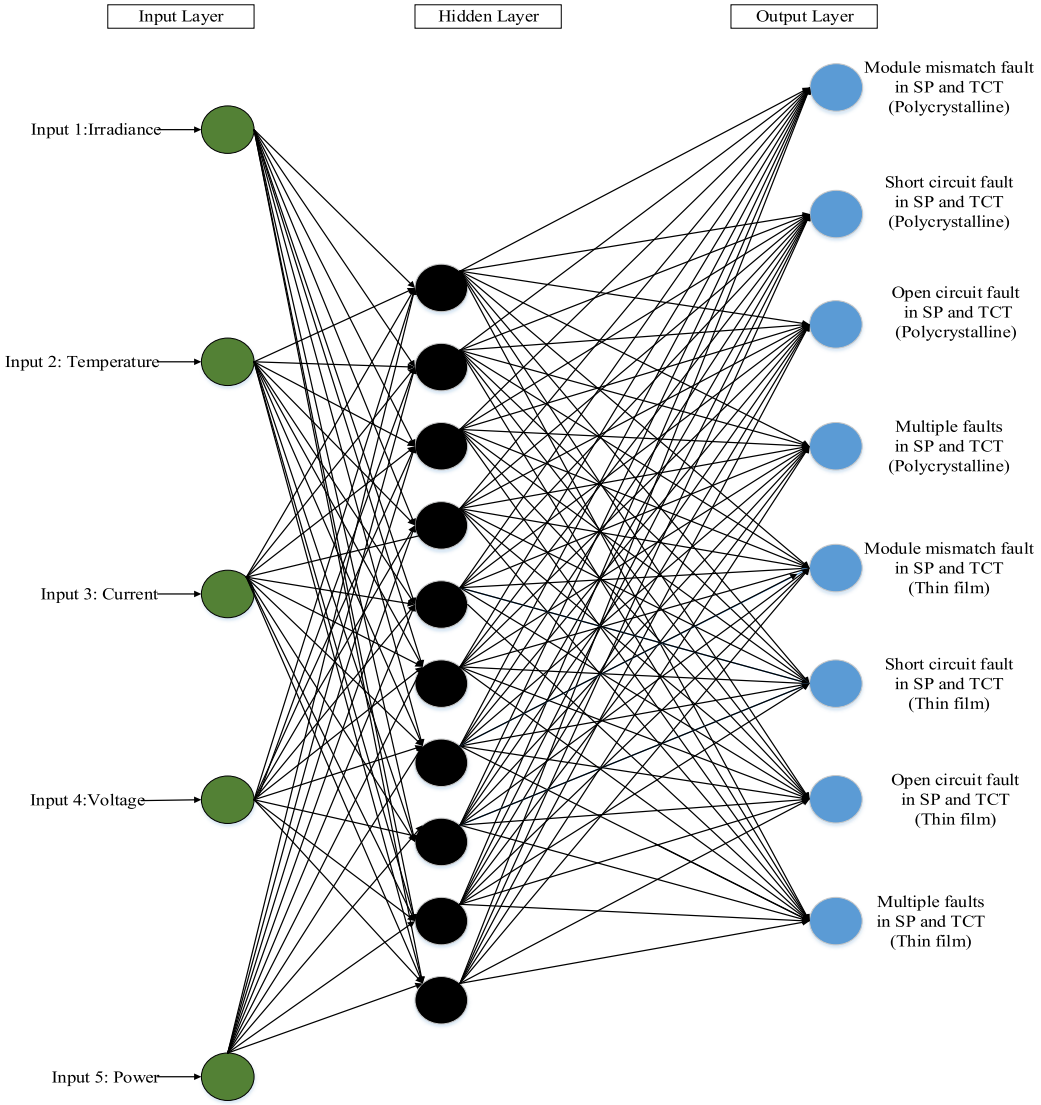

FIGURE 6. Illustration of the developed neural network for classification of PV faults w.r.t PV material.

for training, 15% used for testing, and 15% for validation in training phase of this algorithm. Mean square error (MSE) is used for judgment of performance of algorithm as found in Eq. (12).

$$MSE = \frac{1}{n}\sum_{i=1}^{n}(Y_e - Y_m)^2 \tag{16}$$

where Y_e is estimated, and Y_m is measured values of faults over PV array by the model, respectively.

A. CLASSIFICATION OF FAULTS

The layout of developed neural network is shown in Figure 8. The layout consists of 5 input each having 1248 samples, which propagate to hidden layer of 10 neuron layers to update biases and weights at each iteration. The sigmoid function is used for classification of faults, which constraints the output between 1 and 0. The error is computed by comparing estimated output to the real output, and then biases and weights are updated. The values close to 0 are desirable for estimating correct output. The cross-entropy is a loss function for classification problems. The process can be repeated for specific iterations until global minimum error is achieved.

The data set of 5 × 1248 is collected through characteristic curve analysis and computation of PV parameters after fault occurrence using MATLAB, as shown in Table 2. The 70% of the described data set is used for training, while rest of the 30% data is equally divided for testing and validation of results. These inputs are taken through 5 × 1248 input data set. The output layer consists of 16 outputs that classify data in sixteen different classes of faults. The input parameters of data set are shown in Table 2. All collected input data set 5 × 1248 and target data set of 16 x1248 are then used for categorization of faults in sixteen different classes through training algorithm of SCG.

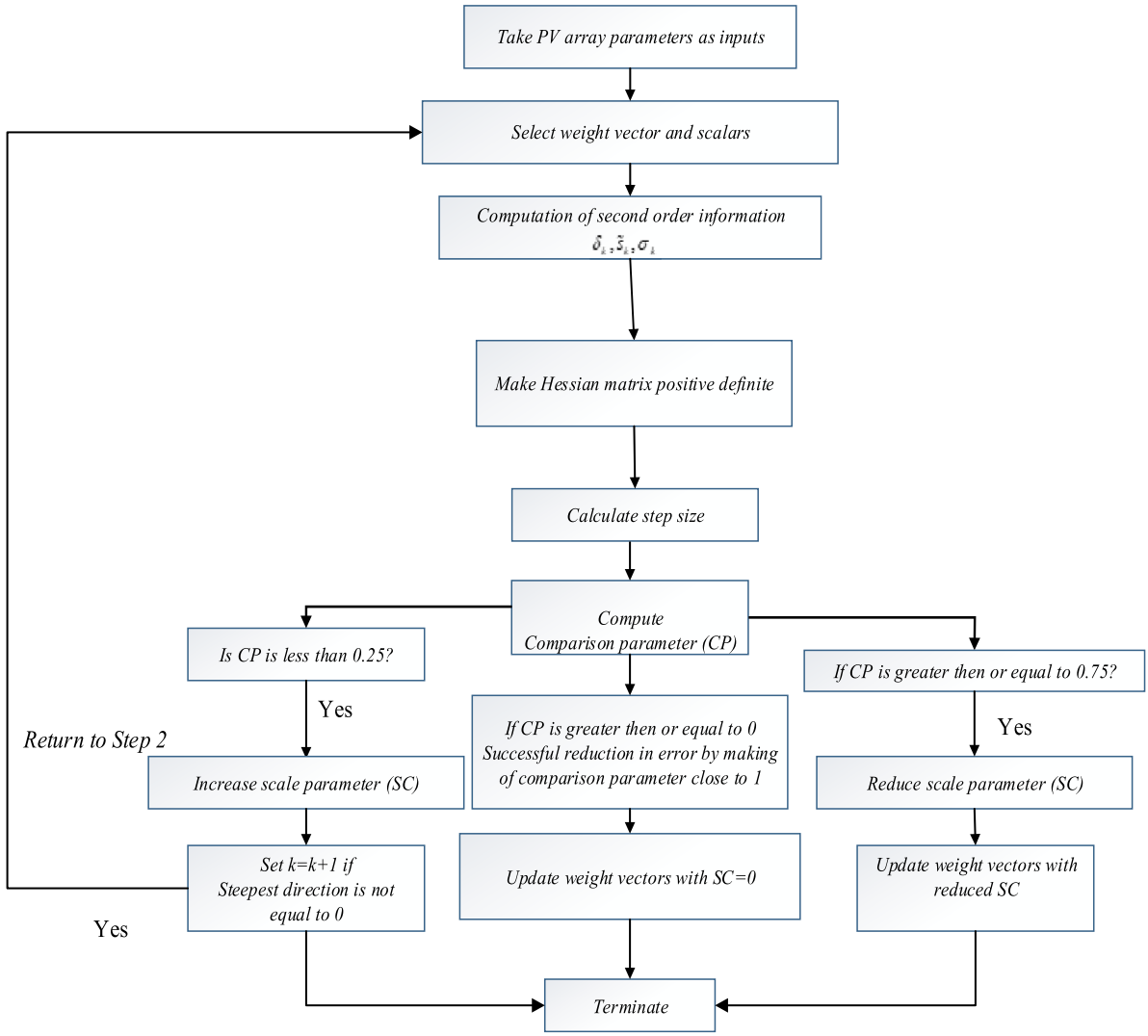

FIGURE 7. SCG algorithm of neural network for fault classification.

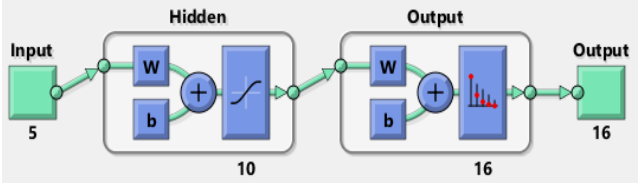

FIGURE 8. Layout of the developed neural network for PV system.

The developed fault scenarios are classified through applying neural network backstage propagation algorithm after analysis of characteristic curve as described above. The obtained graphical results are presented in the next section.

IV. RESULTS AND DISCUSSION

All the developed faults are analyzed through I-V curve analysis in this section. A 9×7 PV array is modeled in MATLAB with a PV module of 150 W each. The technical specifications of the two different PV module, including crystalline module of Ningbosolar electric power and thin-film (a-Si) module of Xunlight, are used for collection of data set as given in Table 3. A total of 9.1 kW power peak is generated in case of no fault operation of the developed 9×7 PV array.

Module Mismatch Fault (F1): The calculated values under this fault are contained in Table 4. Characteristic curve of PV array under fault free operation is shown in Figure 9. Severe partial shading of PV array develops module mismatch fault, as shown in Figure 10. Three interconnections, including TCT, BL, and SP, are compared in terms of characteristic curve. Sudden peak appears in characteristic curve due to unexpected decrease of current. An abrupt reduction in the value of current due to shading indicates a high impact of irradiance on PV array. The change in values of current and voltage reduce power from 9.20 kW to 5.80 kW in total cross-tied, 5.10 kW in bridge-link (BL), and 4.95 kW in

TABLE 2. Considered parameters for input data set.

Input No.	PV parameter
1	Irradiance 'G_R'
2	Temperature 'T_R'
3	Peak Current 'I'
4	Peak Voltage 'V_{oc}'
5	Peak Power 'P'

TABLE 3. Parameters of the studied PV modules.

Open circuit voltage V_{oc} (V)	Short circuit current I_{sc} (A)	Max. peak power P_{max} (W)	Max. peak voltage V_{mp} (V)	Max. peak current I_{mp} (A)
Ningbo Solar electric power TPB125x125 (Polycrystalline PV)				
43.3	4.9	150.0	35.1	4.27
Xunlight XRS18-150 (thin-film PV)				
40.5	6.3	150.0	30.0	5.0
photocurrent I_L (A)	**Diode saturation current I_o (A)**	**Diode ideality factor n**	**Shunt resistance R_{sh} (Ω)**	**Series Resistance R_s (Ω)**
Ningbo Solar electric power TPB125x125 (Polycrystalline PV)				
4.9	6.96e-11	0.943	89.33	0.68
Xunlight XRS18-150 (thin-film PV)				
6.65	1.41e-10	0.95	25.9	1.2

TABLE 4. Computations of PV model for module mismatch fault (F1).

Topology	Peak Power (kW)	Peak voltage (V)	Maximum peak current (A)
		Polycrystalline PV	
TCT	5.8	320	17
BL	5.1	330	15
SP	4.95	326	14
		thin-film PV	
TCT	6.03	275	22
BL	5.8	272	21
SP	5.7	269	19

series-parallel (SP) with multiple peaks in the PV curve, as depicted in Figure 10 and Figure 11. The thin-film PV technology improves the performance in severe shading conditions by decreasing sudden current loss. The power increases from 5.80kW to 6.03 kW in TCT configuration, 5.10kW to 5.80 kW in BL interconnection, and 4.95 kW to 5.70 kW in SP arrangement, respectively.

It is worthwhile to note that the thin-film performs better than polycrystalline with improved power peak. This fault analysis shows that irradiance, temperature are the parameters which have significant impact on power output of PV system

The TCT perform better than other interconnections BL and SP topology in module mismatch fault (F1) and aided in optimizing performance of PV array.

Short Circuit Fault With Bypass Diode Failure (F2): The peak voltage and peak current reduce the power output significantly from 9 kW to 7.2 kW in SP, 6.6 kW in BL and 6.08 kW in TCT configuration as revealed in Figure 12 after occurrence of short circuit fault in PV array. The thin-film

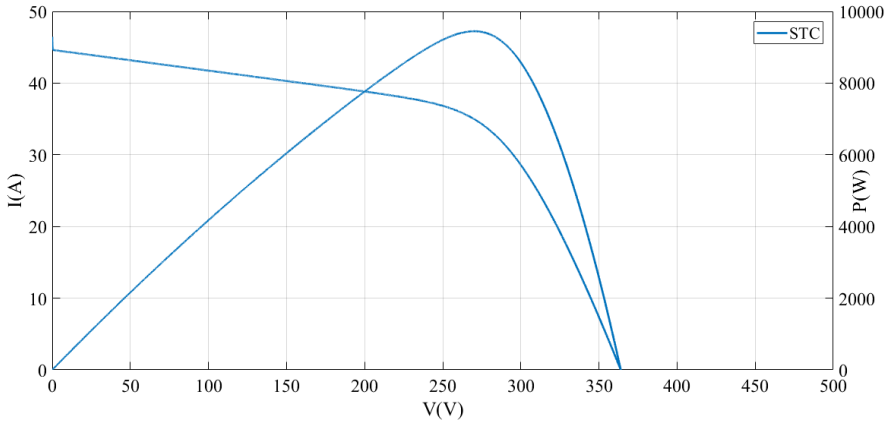

FIGURE 9. Characteristic curve of PV array under the fault free scenario.

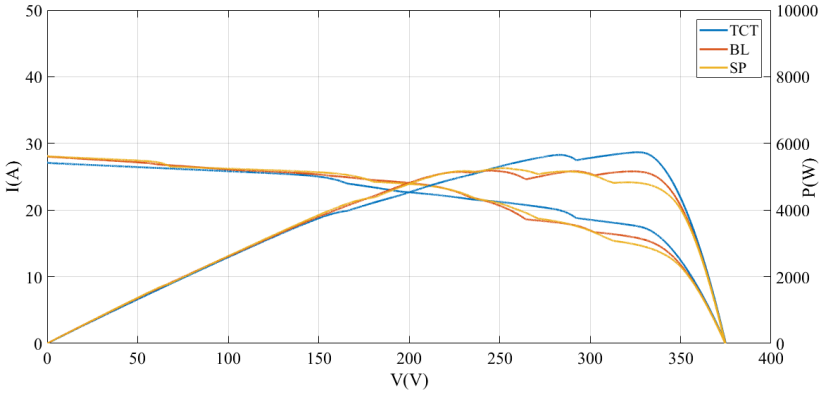

FIGURE 10. Characteristic curve for module mismatch fault (F1) (polycrystalline).

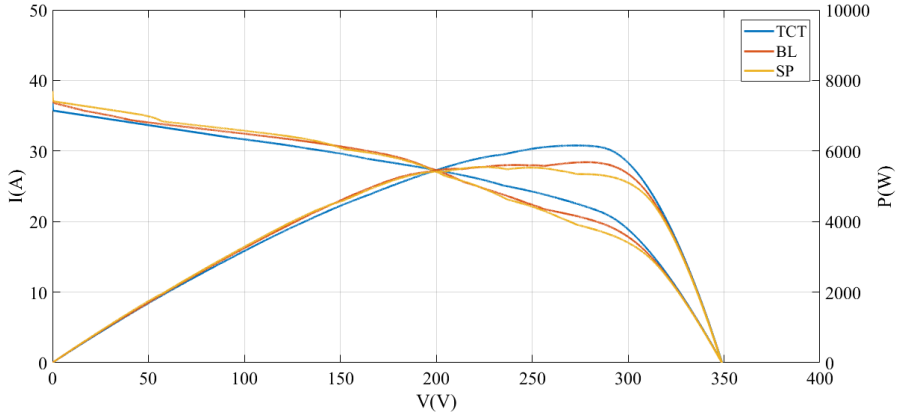

FIGURE 11. Characteristic curve for module mismatch fault 'F1' (TF).

PV array achieves better than poly-crystalline PV array by reducing power loss and increasing power from 7.2 kW to 7.6 kW in SP, 6.6 kW to 7.1 kW in BL interconnections, and 6.08 kW to 6.25 kW in TCT configuration as demonstrated in Figure 13. The computed values of PV model under 'F2' are given in Table 5. The utilization of thin-film can improve the power loss minimization and optimize the system's performance, but still, power loss occurs in both PV arrays.

The SP arrangement accomplishes better than the other interconnections under 'F2' scenario and indicates that

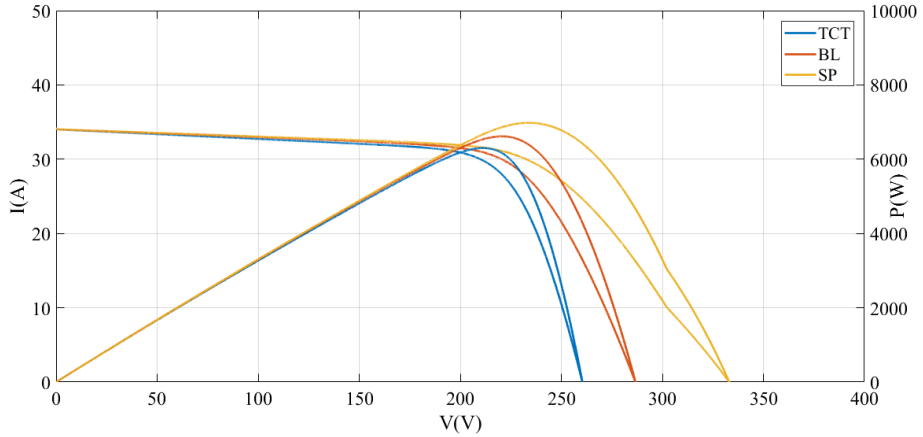

FIGURE 12. Characteristic curve for short circuit fault (F2) (Polycrystalline).

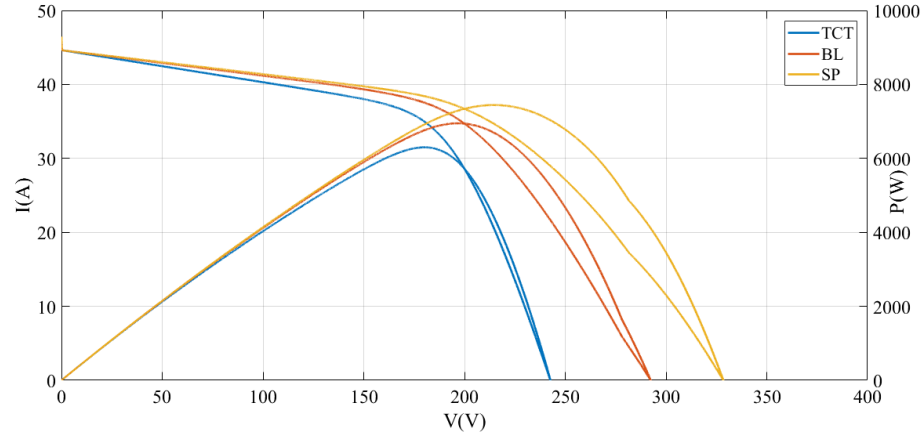

FIGURE 13. Characteristic curve for short circuit fault (F2) (TF).

TABLE 5. Computations of the PV model during short circuit fault (F2).

Topology	Max. peak power (kW)	Max. peak voltage (V)	Max. peak current (A)
		Polycrystalline PV	
TCT	6.08	210	30
BL	6.60	221	31
SP	7.21	235	31.5
		Thin-film PV	
TCT	6.25	180	34.9
BL	7.12	200	36.5
SP	7.6	217	37.8

selection of suitable interconnection can impact the performance of PV system.

Enhanced peak power is attained in SP configuration than that of TCT and BL interconnections with the use of of thin-film (a-Si) PV technology, as evident from Figure 13.

Open Circuit Fault (F3): As depicted in Figure 14 and Figure 15, TCT interconnection outperforms the other interconnections with minimization of power loss and significant current loss. In with polycrystalline PV, maximum peak power increases from 8 kW of SP to 8.69 kW in TCT and

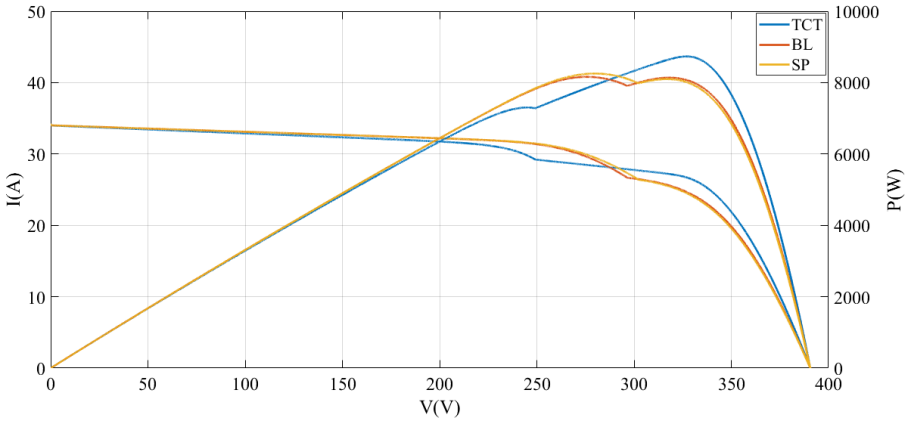

FIGURE 14. Characteristic curve for open circuit fault (F3) (Polycrystalline).

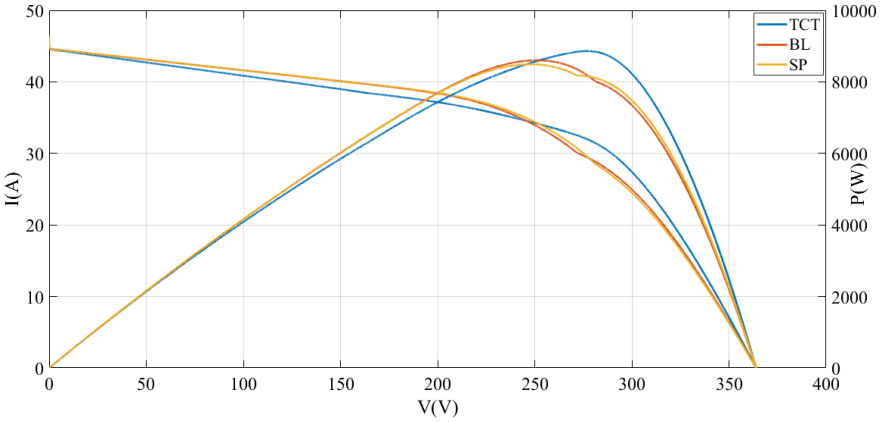

FIGURE 15. Characteristic curve for open circuit fault (F3) (TF).

TABLE 6. Computations of PV model for open circuit fault (F3).

Topology	Max. peak power (kW)	Max. peak voltage (V)	Max. peak current (A)
		Polycrystalline PV	
TCT	8.6	310	27.2
BL	8.1	320	24
SP	8.0	310	23
		Thin-film PV	
TCT	8.8	272	36
BL	8.45	250	34.5
SP	8.3	250	34

8.1 kW of BL. Computed values of PV model under (F3) are given in Table 6. It is seen that thin-film does better than polycrystalline under this fault situation, as shown in the curve analysis.

Impact of Multiple Faults (F4): It is conducted for analysis of performance of all adopted interconnection with thin-film and crystalline material. The power reduced from 8 kW to 5.0 kW in SP, 4.85 kW in BL, and 5.0kW in TCT interconnections with polycrystalline PV array, as illustrated in Figure 16 and Figure 17. Computed values of the PV system under multiple fault scenario are given in Table 7.

The produced power decreased from 8kW to 5.21kW in SP interconnection, 5.4 kW in BL, and 5.3 kW in TCT with thin-film PV technology, as revealed in Figure 16.

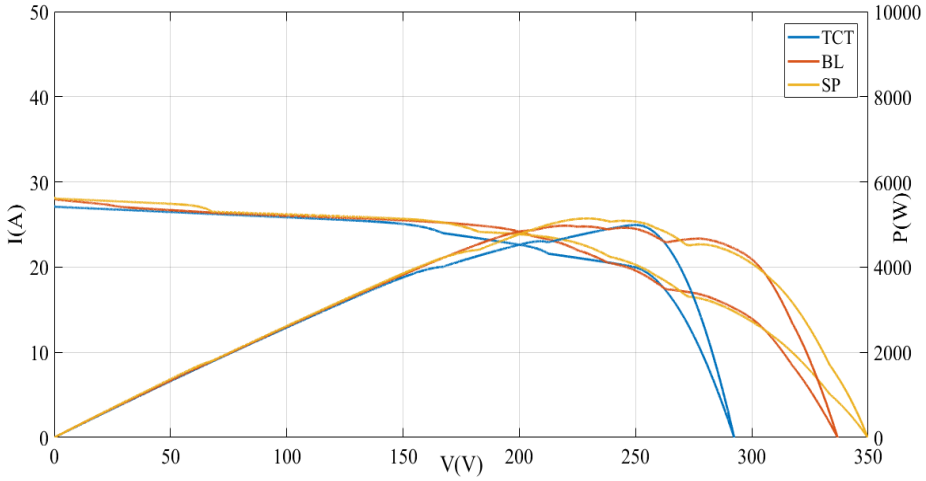

FIGURE 16. Characteristic curve for multiple fault (F4) (polycrystalline).

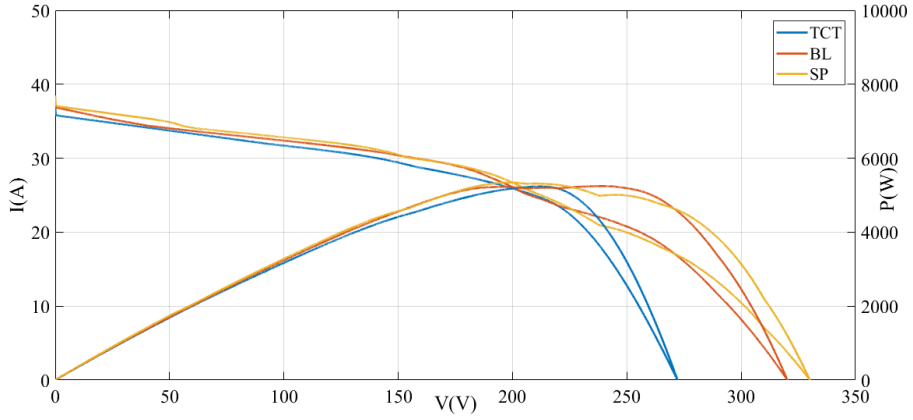

FIGURE 17. Characteristic curve for multiple fault (F4) (TF).

TABLE 7. Computations of PV model under multiple faults (F4).

Topology	Max. peak power (kW)	Max. peak voltage (V)	Max. peak current (A)
		Polycrystalline PV	
TCT	5.0	250	20.3
BL	4.85	250	19.6
SP	5.01	250.1	20.4
		Thin-film PV	
TCT	5.21	215	24
BL	5.4	250	25
SP	5.3	228	23

The thin-film PV array performs better than polycrystalline in all developed fault cases. A data set of 5×1170 is generated through computing and analyzing parameters of developed PV model. All considered faults are then classified and categorized through DNN in next section.

A. RESULTS FOR CLASSIFICATION OF PV FAULTS

The input data consisting of PV parameters is trained over 101 iterations with NN. The results are evaluated in terms of cross-entropy (CE), which specifies that the minimum global error (MGE) is accomplished. The data set is trained through

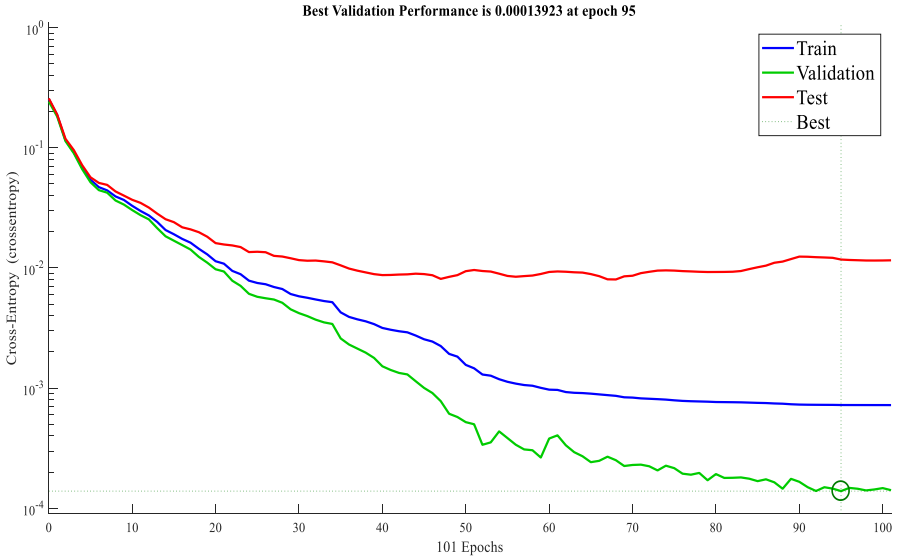

FIGURE 18. Graph showing best performance validation at epoch 95.

SCG algorithm, and performance is measured through plotting confusion matrix, ROC plot analysis, and validation of performance through plotting cross-entropy (CE) with number of epochs. The best validation performance is indicated by plotting cross-entropy (CE) of training, testing, and validation data on Y-axis with number of iterations on X-axis, as shown in Figure 18. The performance is computed for each epoch, and best performance is chosen at a point when all coincide at same point. At that point in time, the training should be stopped, and no further iterations should be proceeded. It means that no further training is required, and if done, it may mispredict the results. The greatest validation presentation is 0.0001392 at epoch 95, as depicted in Figure 18. This graph shows the value of achieved cross-entropy (CE) for each iteration. The less value of CE indicates proper classification and less error in classification of faults, which is achieved by this NN classification. The X-axis and Y-axis indicate the number of iterations, i.e., 101 epochs and CE for each iteration, respectively. The phenomenon of overfitting is also indicated in the graph due to difference in the value of cross-entropy for training and testing data at epoch 101.

Training states are shown in Figure 19 in which first plot shows less value of gradient '0.37929e-05' at epoch 101, which indicates the network is learning up to a great extent due to reasonable adjustment of the weights and biases. The proper adjustment in weights and bias make the network more reliable and increase the chances of accurate classification. The validation plot shows the six validation checks at epoch 101. This plot shows the points where failure across certain limit is an endpoint for training, indicating the start of overfitting of data. Failure of values after epoch 50 can be seen where overfitting of data is also started, as shown in Figure 19. The plots show the variation of gradient error, which is 0.37929e-05 at epoch 101, and number of validation checks are six at epoch 101.

The confusion matrix indicates successful classification of sixteen different fault classes, including with accuracy of 99.6%, as shown in Figure 20. The confusion matrix indicates successful classification of sixteen different classes of faults including 1) module mismatch in polycrystalline with SP, 2) short circuit in polycrystalline with SP, 3) open circuit in polycrystalline with SP, 4) multiple faults in polycrystalline with SP, 5) module mismatch in thin-film with SP, 6) short circuit in thin-film with SP, 7) open circuit in thin-film with SP, 8) multiple faults in thin-film with SP, 9) module mismatch in polycrystalline with TCT, 10) short circuit in polycrystalline with TCT, 11) open circuit in polycrystalline with TCT, 12) multiple faults in polycrystalline with TCT, 13) module mismatch in thin-film with TCT, 14) short circuit in thin-film with TCT, 15) open circuit in thin-film with TCT, 16) multiple faults in thin-film with TCT, with accuracy of 99.6%. Diagonal element of matrix represents the correctly predicted samples. The classification of faults in sixteen different classes is shown in Table 8.

The training data is used for determining the weights and thresholds of the PV models given input and targets data set. The validation data set is a non-training set whereas testing data is a set of data that indicates the unbiased performance estimates. Separate confusion matrix is plotted for all three data sets, as shown in Figure 20, which describe the performance of classification model. It permits the conception of training algorithm's performance through identification of confusion between different classes. Information about overfitting of data can also be extracted by using confusion matrix. Significant difference in the results of training and testing data can indicate overfitting of data, as indicated in Figure 20 and Figure 22. Nearly 96.6% accuracy is achieved in predicting class 1 fault for training data, as shown in Figure 20, while 75% accuracy is achieved in predicting class 1 for testing data, as shown in Figure 22. All the remaining classes

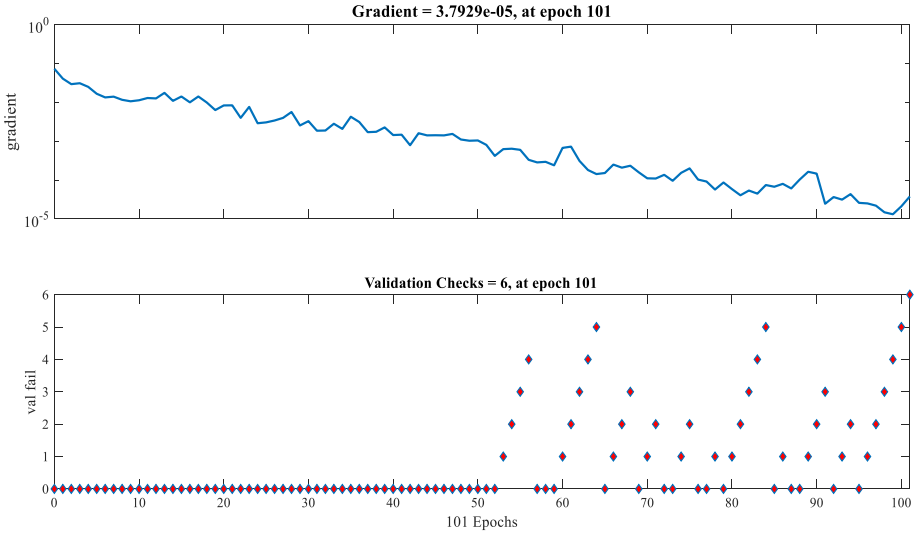

FIGURE 19. Plot showing training state.

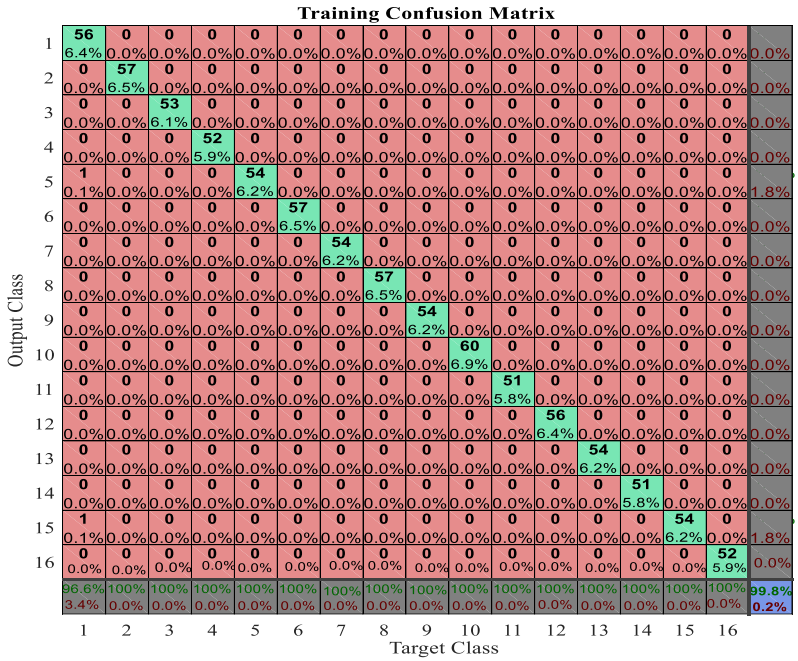

FIGURE 20. Training Confusion matrix for 16 classes of fault indicating CF1-CF16.

are successfully predicted for both training and testing data, as shown in Figure 20-22.

The rows correspond to the predicted fault class, i.e., output fault class, while column corresponds to target fault class. The diagonal cells denote the correctly classified classes, while off-diagonal values are incorrectly classified or confused classes.

1) True positive (TP): accurately foreseen faulty classes
2) True negative (TN): accurately foreseen non-faulty classes
3) False positive (FP): Incorrectly predicted fault classes, which means they do not belong to that class.
4) False negative (FN): Incorrect prediction of non-faulty class, which means that they belong to that fault class but misclassified. The error histogram indicates very less error in classification of faults, as shown in Figure 22. The histogram shows very less error in classification of faults, i.e., 0.007901 in testing, validation, and training samples.

Confusion matrix is used for describing and evaluating the performance of classifier on the test data while the ROC graph summarizes the confusion matrices generated for each threshold without having actual calculation of them. In other words, Receiver Operator Characteristic Curve can assist in

TABLE 8. Classification of PV faults in different classes.

Classes	PV faults
CF1	Module mismatch (polycrystalline) in SP
CF2	Short circuit (polycrystalline) in SP
CF3	Open circuit (polycrystalline) in SP
CF4	Multiple faults (polycrystalline) in SP
CF5	Module mismatch (thin-film) in SP
CF6	Short circuit (thin-film) in SP
CF7	Open circuit (thin-film) in SP
CF8	Multiple faults (thin-film) in SP
CF9	Module mismatch (polycrystalline) in TCT
CF10	Short circuit (polycrystalline) in TCT
CF11	Open circuit (polycrystalline) in TCT
CF12	Multiple faults (polycrystalline) in TCT
CF13	Module mismatch (thin-film) in TCT
CF14	Short circuit (thin-film) in TCT
CF15	Open circuit (thin-film) in TCT
CF16	Multiple faults (thin-film) in TCT

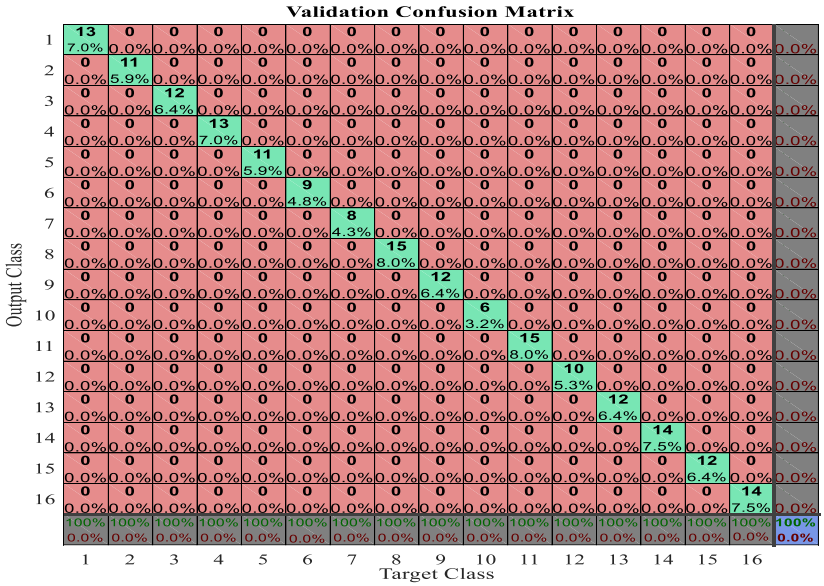

FIGURE 21. Validation confusion matrix for 16 classes of fault indicating CF1-CF16.

determining the value of best threshold. Confusion matrix and ROC are selected for assessing the classification capabilities of the trained NN classifier in this study. A confusion matrix gives a complete picture about performance of classifier and allows computation of various classification metrics, which is the main reason for selecting confusion matrix with ROC to assess the performance of proposed neural network training algorithm. Confusion matrix is best performance evaluation of multiclass problems. The results of region of convergence (ROC) are given in Figure 23. The ROC uses two parameters including false and true positive rate sensitivities with various thresholds for showing performance

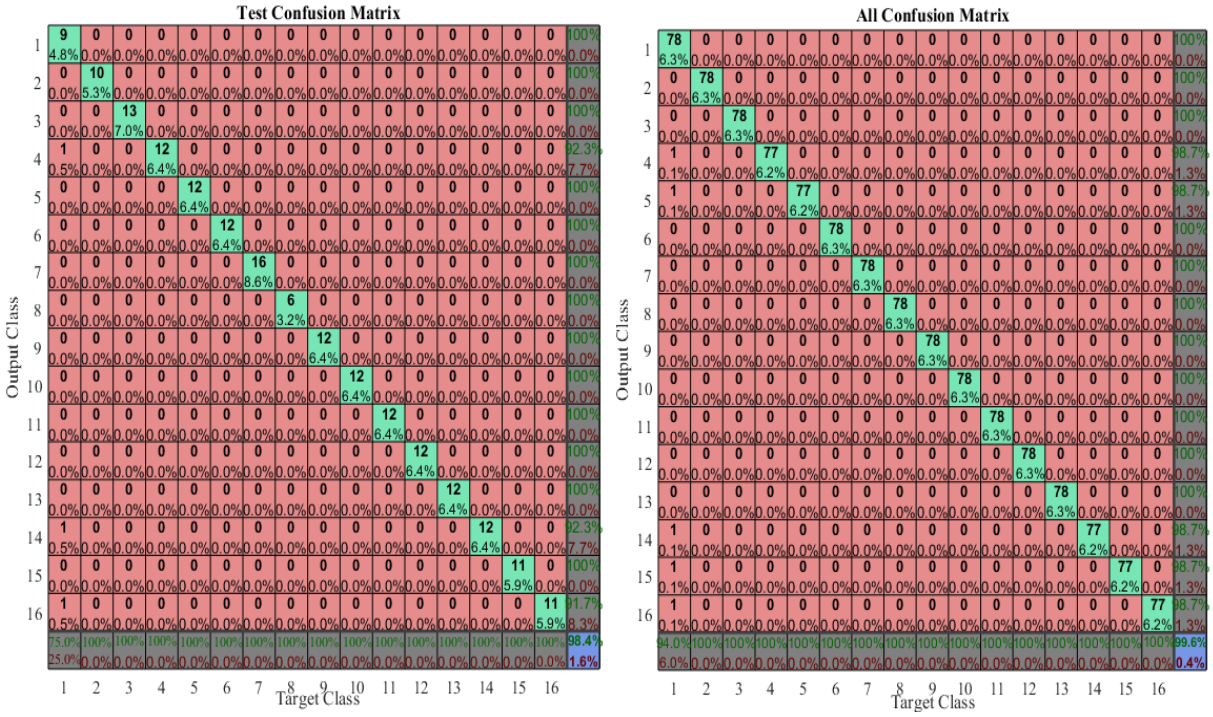

FIGURE 22. Classification of sixteen different fault classes via test confusion matrix and all confusion matrix.

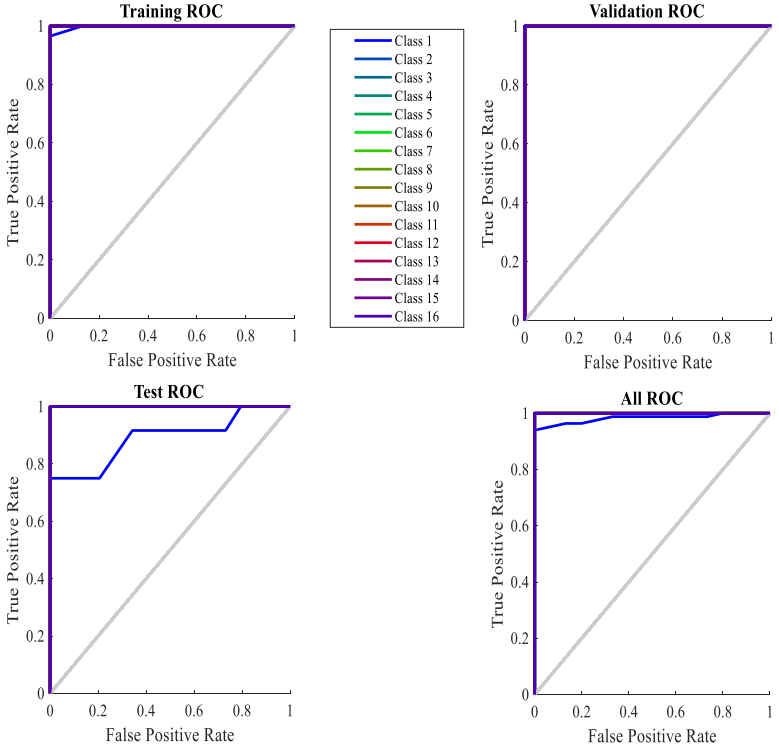

FIGURE 23. Results of ROC for accurate fault classification.

of classification model. All results are also given for accurate evaluation of results, as shown in Table 9 and Table 10. The low values of Cross entropy (CE) near zero indicate proper classification. The Percentage error indicates misclassified fraction of sample. The value close to 0 means very less fraction of misclassified samples, which is desirable. Sensitivity and specificity are two measures of fault prediction model. Sensitivity is denoted by True Positive

TABLE 9. Comparison of the presented results with literature works.

Case study	Algorithm	Accuracy of computed results	Misclassification rate	Objective
Proposed work	Multilayer neural network based on Scaled Conjugate Gradient	99.6%	0.4%	Classification of PV faults in 16 different classes (different PV configurations and materials like thin-film and crystalline)
[18]	Detection of shading fault based on I-V curve through principal component analysis	97%	3%	Classification of shading fault in four different classes
[20]	Health monitoring of PV array based on PNN	98.53%	1.47%	Classification of short circuit and open circuit faults
[19]	Convolutional neural network (CNN) for fault detection through 2D scalograms	73.5% with CNN	26.8%	Classification of PV faults in 5 different classes
[24]	Diagnosis of faults through I-V measurements with machine learning techniques, multiclass exponential loss function (SAM E-CART)	Above 95% average accuracy (different accuracy in each case)	Less than 5%	Diagnosis of short circuit, open circuit, abnormal aging, and bypass diode faults
[21]	SA-RBF kernel extreme learning for fault diagnosis	96.9% trainıng accuracy and 93.5% testing accuracy	3.1% training and 6.5% testing	Classification of short circuıt, shading, and aging fault
[13]	Probabilistic neural network (PNN)	85%	15%	Classification of short circuit, aging and shading faults
[22]	Detection of shading through NN in partially shaded PV modules	High accuracy with 0.998 correlation coefficient	Very less error rate (0.01 MSE)	Detect shading of modules through regression analysis

Rate (TPR), which is proportion of correctly identified class. It means a correctly classified fault among fault positive population (Class = 1) represented as Eq. (13).

$$Sensitivity = TPR = \frac{TP}{TP + FN} \tag{17}$$

Specificity is a measure of True Negative Rate which denotes the percentage of the known negatives among the fault negative population (class = 0) denoted as Eq. (14).

$$Specificity = \frac{TN}{TN + FP} \tag{18}$$

False Positive Rate (FPR) is a proportion of identified positive (identified faults) among the population which does not belong to that fault class. It is equal to 1-specificity. Specificity Sensitivity, which is the True Positive Rate amongst the diabetes-positive population. Sensitivity = True Positives/(True Positives + False Negatives). The overall performance can be evaluated by area under the curve in the region of convergence (ROC) plot as shown in Figure 23. It represents the ability of classification algorithm to distinguish 1s (positives) from 0s (negatives).the plot shows the accurate classification as results of both specificity and sensitivity are close to 1 indicating 99.6% accuracy of fault's classification.

$$Accuracy = \frac{TP + TN}{TP + FN + TN + FP} = 99.6\% \tag{19}$$

The ROC plot shows points in the upper left corner indicating the accurate classification of 8 fault classes with 99.6% sensitivity and specificity. More accuracy than test ROC is achieved in predicting class 1 fault for train ROC as shown in Figure 23. All remaining classes are successfully predicted for both train ROC and test ROC. The same results are observed in the confusion matrix, which also shows overfitting of data for predicting faults in both classifiers.

A comparison of the presented results with that of literature works is shown in Table 9. All faults are accurately

TABLE 10. Computation of error and cross-entropy in samples.

Results	Samples	Cross Entropy (CE)	%Error
Training	874	5.78017e-0	1.14416e-1
Validation	187	16.44026e-0	0
Testing	187	16.39030e-0	8.02139e-1

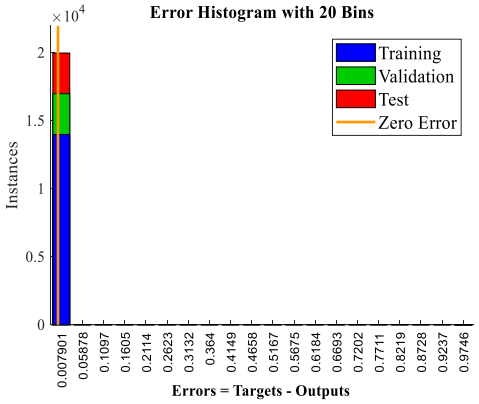

FIGURE 24. Error histogram indicating error in the classification of faults.

classified in sixteen different classes with 99.6% accuracy. None of the previous research has classified faults in different PV configurations and materials, which is a significant contribution of this study. The confusion matrix clearly shows that 99.6% accuracy of classification and 0.4% misclassification rate in prediction of fault classes. Different PV materials are also differentiated in the classification faults. Sixteen different classes of faults are differentiated based on irradiance, temperature of individual PV modules, open circuit voltage, short circuit current, and generated peak power. Table 10 shows the computation of errors and cross-entropy in separate samples of the data set. The 1248 samples of five inputs are separated into 874 samples for training, which achieved CE of 5.78017e-0 and error of 1.14416e-1 %, 187 samples for validation, and 187 samples for testing which achieved 16.44026e-0 and 16.39030e-0 values of CE respectively. Approximately 0% and 8.02e-1 % of errors are achieved by validation and testing data, respectively. Low values of CE indicate excellent performance, which is achieved by this training algorithm. The low value of error indicates the reduced misclassification rate, which is desirable for proper classification of faults.

V. CONCLUSION

In this study, various types of PV faults, including module mismatch fault, open circuit, short circuit, and multiple faults under partial shading, are classified in SP, and TCT interconnections made of polycrystalline and thin-film PV arrays through multilayer neural network (MNN). To be extensive in the research study, a large input data set of 5×1248 and target data set of 16×1248 are developed for categorization of faults in sixteen different classes of PV faults. The characteristic curve of three different configurations of 9×7 PV array, including SP, BL, and TCT, is analyzed for analysis of the impact of faults on various parameters of PV array like short and, open circuit voltage, and peak power etc. The SCG training algorithm classified all the developed faults in thin-film and polycrystalline PV materials with high accuracy of 99.6% and a fast-computational time of 0.08 sec, which is not reported in the related literature.

The results are validated through plotting best validation performance, confusion matrix, and region of convergence (ROC) analysis for classification of faults in different PV technologies, which may be considered a unique attempt of the presented research study. The ROC plot and confusion matrix plot show the 99.6% accuracy with fast computational time of 0.08 sec. This research work does not only help timely diagnosis of PV faults but also categorizes them in two different PV materials, which may lead towards the longer lifespan and better performance of a PV system. Classification of faults in crystalline and thin-film PV configurations with high accuracy is performed in the proposed work. Further research is needed to classify faults like thin cracks of crystalline and thin-film PV modules using advanced techniques. Practical implementation of proposed work can also be considered as a future enhancement of the proposed work. The proposed method can be implemented via low-cost microcontrollers for real-time applications.

ACKNOWLEDGMENT

This project was funded by the Deanship of Scientific Research (DSR), King Abdulaziz University, Jeddah, under grant No. (D-639-135-1441). The authors, therefore, gratefully acknowledge DSR technical and financial support.

REFERENCES

[1] M. A. Hejazi, "The comprehensive study of electrical faults in PV arrays," *J. Electr. Comput. Eng.*, vol. 2016, p. 10, Dec. 2016.

[2] M. K. Alam, F. Khan, J. Johnson, and J. Flicker, "A comprehensive review of catastrophic faults in PV arrays: Types, detection, and mitigation techniques," *IEEE J. Photovolt.*, vol. 5, no. 3, pp. 982–997, May 2015.

[3] A. Mehiri, A.-K. Hamid, and S. Almazrouei, "The effect of shading with different PV array configurations on the grid-connected PV system," in *Proc. Int. Renew. Sustain. Energy Conf. (IRSEC)*, Dec. 2017, pp. 1–6.

[4] L. Schirone, F. P. Califano, and M. Pastena, "Fault detection in a photovoltaic plant by time domain reflectometry," *Prog. Photovolt., Res. Appl.*, vol. 2, no. 1, pp. 35–44, Jan. 1994.

[5] T. I. Takashima, J. Yamaguchi, K. Otani, T. Oozeki, K. Kato, and M. Ishida, "Experimental studies of fault location in PV module strings," *Sol. Energy Mater. Sol. Cells*, vol. 93, pp. 1079–1082, Jun. 2009.

[6] P. S. Wang and S. C. Zheng, "Fault analysis of photovoltaic array based on infrared image," *Acta Energiae Solaris Sinica*, vol. 31, no. 2, pp. 197–201, 2010.
[7] T. Takashima, J. Yamaguchi, and M. Ishida, "Disconnection detection using Earth capacitance measurement in photovoltaic module string," *Prog. Photovolt., Res. Appl.*, vol. 16, no. 8, pp. 669–677, Dec. 2008.
[8] H. Patel and V. Agarwal, "MATLAB-based modeling to study the effects of partial shading on PV array characteristics," *IEEE Trans. Energy Convers.*, vol. 23, no. 1, pp. 302–310, Mar. 2008.
[9] R. A. Kumar, R. K. Pachauri, and Y. K. Chauhan, "Experimental analysis of SP/TCT PV array configurations under partial shading conditions," in *Proc. IEEE 1st Int. Conf. Power Electron., Intell. Control Energy Syst. (ICPEICES)*, Delhi, India, Jul. 2016, pp. 1–6.
[10] K. M. Chao, S.-H. Ho, and M.-H. Wang, "Modeling and fault diagnosis of a photovoltaic system," *Electr. Power Syst. Res.*, vol. 78, no. 1, pp. 97–105, 2008.
[11] X. H. Nguyen, "MATLAB/Simulink based modeling to study effect of partial shadow on solar photovoltaic array," *Environ. Syst. Res.*, vol. 4, no. 1, p. 20, Dec. 2015.
[12] S. Gul, A. Ul Haq, M. Jalal, A. Anjum, and I. U. Khalil, "A unified approach for analysis of faults in different configurations of PV arrays and its impact on power grid," *Energies*, vol. 13, no. 1, p. 156, Dec. 2019.
[13] L. Chen, W. Han, Y. Huang, and X. Cao, "Online fault diagnosis for photovoltaic modules based on probabilistic neural network," *Eur. J. Electr. Eng.*, vol. 21, no. 3, pp. 317–325, Aug. 2019.
[14] S. Samara and E. Natsheh, "Intelligent real-time photovoltaic panel monitoring system using artificial neural networks," *IEEE Access*, vol. 7, pp. 50287–50299, 2019.
[15] Y. H. Sabry, W. Z. W. Hasan, A. H. Sabry, M. Z. A. A. Kadir, M. A. M. Radzi, and S. Shafie, "Measurement-based modeling of a semi-transparent CdTe thin-film PV module based on a custom neural network," *IEEE Access*, vol. 6, pp. 34934–34947, 2018.
[16] S. Laamami, M. Benhamed, and L. Sbita, "Artificial neural network- based fault detection and classification for photovoltaic system," in *Proc. Int. Conf. Green Energy Convers. Syst. (GECS)*, Mar. 2017, pp. 978–984.
[17] V. S. B. Kurukuru, A. Haque, M. A. Khan, and A. K. Tripathy, "Fault classification for photovoltaic modules using thermography and machine learning techniques," in *Proc. Int. Conf. Comput. Inf. Sci. (ICCIS)*, Apr. 2019, pp. 1–6.
[18] S. Fadhel, C. Delpha, D. Diallo, I. Bahri, A. Migan, M. Trabelsi, and M. F. Mimouni, "PV shading fault detection and classification based on I-V curve using principal component analysis: Application to isolated PV system," *Sol. Energy*, vol. 179, pp. 1–10, Feb. 2019.
[19] M. N. Akram and S. Lotfifard, "Modeling and health monitoring of DC side of photovoltaic array," *IEEE Trans. Sustain. Energy*, vol. 6, no. 4, pp. 1245–1253, Oct. 2015.
[20] F. Aziz, A. Ul Haq, S. Ahmad, Y. Mahmoud, M. Jalal, and U. Ali, "A novel convolutional neural network-based approach for fault classification in photovoltaic arrays," *IEEE Access*, vol. 8, pp. 41889–41904, 2020.
[21] Y. Wu, Z. Chen, L. Wu, P. Lin, S. Cheng, and P. Lu, "An intelligent fault diagnosis approach for PV array based on SA-RBF kernel extreme learning machine," *Energy Procedia*, vol. 105, pp. 1070–1076, May 2017.
[22] H. Mekki, A. Mellit, and H. Salhi, "Artificial neural network-based modelling and fault detection of partial shaded photovoltaic modules," *Simul. Model. Pract. Theory*, vol. 67, pp. 1–13, Sep. 2016.
[23] M. A. Mannan and M. A. Anjan, "Modeling of current-voltage characteristics of thin film solar cells," *Solid State Electron.*, vol. 63, pp. 49–54, Sep. 2011.
[24] J.-M. Huang, R.-J. Wai, and W. Gao, "Newly-designed fault diagnostic method for solar photovoltaic generation system based on IV-curve measurement," *IEEE Access*, vol. 7, pp. 70919–70932, 2019.
[25] A. Chouder and S. Silvestre, "Automatic supervision and fault detection of PV systems based on power losses analysis," *Energy Convers. Manage.*, vol. 51, no. 10, pp. 1929–1937, Oct. 2010.
[26] A. S. W. Drews, "Monitoring and remote failure detection of grid-connected PV systems based on satellite observations," *Sol. Energy*, vol. 81, no. 4, pp. 548–564, Apr. 2007.
[27] S. K. Firth, K. J. Lomas, and S. J. Rees, "A simple model of PV system performance and its use in fault detection," *Sol. Energy*, vol. 84, no. 4, pp. 624–635, Apr. 2010.
[28] D. A. Quansah and M. S. Adaramola, "Comparative study of performance degradation in poly- and mono-crystalline-Si solar PV modules deployed in different applications," *Int. J. Hydrogen Energy*, vol. 43, no. 6, pp. 3092–3109, Feb. 2018.
[29] B. Dhanalakshmi and N. Rajasekar, "Dominance square based array reconfiguration scheme for power loss reduction in solar PhotoVoltaic (PV) systems," *Energy Convers. Manage.*, vol. 156, pp. 84–102, Jan. 2018.
[30] I. U. Khalil, A. Ul-Haq, Y. Mahmoud, M. Jalal, M. Aamir, M. U. Ahsan, and K. Mehmood, "Comparative analysis of photovoltaic faults and performance evaluation of its detection techniques," *IEEE Access*, vol. 8, pp. 26676–26700, 2020.
[31] S. Padmanaban, N. Priyadarshi, J. B. Holm-Nielsen, M. S. Bhaskar, F. Azam, A. K. Sharma, and E. Hossain, "A novel modified sine-cosine optimized MPPT algorithm for grid integrated PV system under real operating conditions," *IEEE Access*, vol. 7, pp. 10467–10477, 2019.
[32] X. Sun, T. Silverman, R. Garris, C. Deline, and M. A. Alam, "An illumination- and temperature-dependent analytical model for copper indium gallium diselenide (CIGS) solar cells," *IEEE J. Photovolt.*, vol. 6, no. 5, pp. 1298–1307, Sep. 2016.
[33] S. R. Pendem and S. Mikkili, "Performance evaluation of series, series-parallel and honey-comb PV array configurations under partial shading conditions," in *Proc. 7th Int. Conf. Power Syst. (ICPS)*, Dec. 2017, pp. 749–754.
[34] P. K. Bonthagorla and S. Mikkili, "A novel fixed PV array configuration for harvesting maximum power from shaded modules by reducing the number of cross-ties," *IEEE J. Emerg. Sel. Topics Power Electron.*, early access, Mar. 9, 2020, doi: 10.1109/JESTPE.2020.2979632.

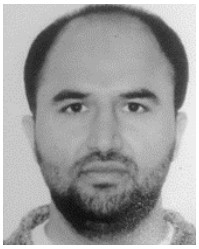

AZHAR UL-HAQ received the Ph.D. degree in electrical engineering from the Joint Research Doctoral Program, University of L'Aquila, Italy, and the University of Waterloo, Canada. He worked as a Research Assistant at the ECE Department, University of Waterloo, in 2015. He has been working as an Assistant Professor at the Department of Electrical Engineering, National University of Sciences and Technology, Islamabad, since October 2016. His research interests include grid integration of renewable energies, PV powered smart charging of electric vehicles, and direct load control strategies for peak-shaving in power systems.

HATEM F. SINDI (Member, IEEE) received the B.Sc. degree in electrical engineering from King Abdulaziz University, Jeddah, Saudi Arabia, in 2007, and the M.Sc. and Ph.D. degrees in electrical engineering from the University of Waterloo, Waterloo, ON, Canada, in 2013 and 2018, respectively. He is currently an Assistant Professor with the Department of Electrical and Computer Engineering, King Abdulaziz University. His research interests include smart grids, renewable DG, distribution system planning, electric vehicles, storage systems, and bulk power system reliability.

SABA GUL received the B.S. degree in electronic engineering from the Sir Syed University of Engineering and Technology, Pakistan, in 2017, and the M.S. degree in power and control systems from the College of Electrical and Mechanical Engineering, National University of Sciences and Technology (NUST), Islamabad, Pakistan. Her research interests include impact of renewable energy integration and power system stability issues.

MARIUM JALAL received the Ph.D. degree in electrical engineering from the University of L'Aquila, Italy, in April 2015. From 2011 to 2014, she was a Marie-Curie Early Stage Researcher with the Center of Excellence for Research DEWS, University of L'Aquila. Her research interests include smart grid technologies and energy efficiency techniques in smart cities. She was a recipient of several research and travel grant awards. She was awarded with the Gold Medal for the Best M.Sc. Thesis from LCWU, Lahore.